Choked Flow Effects in the NSI Driven Pin Puller*

Keith A. Gonthier† and Joseph M. Powers‡

Department of Aerospace and Mechanical Engineering
University of Notre Dame
Notre Dame, Indiana 46556-5637

Abstract

This paper presents an analysis for pyrotechnic combustion and pin motion in the NASA Standard Initiator (NSI) actuated pin puller. The conservation principles and constitutive relations for a multi-phase system are posed and reduced to a set of eight ordinary differential equations which are solved to predict the system performance. The model tracks the interactions of the unreacted, incompressible solid pyrotechnic, incompressible condensed phase combustion products, and gas phase combustion products. The model accounts for multiple pyrotechnic grains, variable burn surface area, and combustion product mass flow rates through an orifice located within the device. Pressure-time predictions compare favorably with experimental data. Results showing model sensitivity to changes in the cross-sectional area of the orifice are presented.

Introduction

Pyrotechnically actuated devices are widely used for aerospace applications. Examples of such devices are pin pullers, exploding bolts, and cable cutters. Full-scale modeling efforts of pyrotechnically driven systems are hindered by many complexities: three dimensionality, time-dependency, complex reaction kinetics, *etc.* Consequently, simple models have been the preferred choice of many researchers.[1,2,3,4] These models require that a number of assumptions be made; typically, a well stirred reactor is simulated; also, the combustion product composition is typically predicted using principles of equilibrium thermochemistry, and the combustion rate is modeled by a simple empirical expression.

Recently, Gonthier and Powers[5] described a methodology for modeling pyrotechnic combustion driven systems which is based upon principles of mixture theory. Though this approach still requires that simplifying assumptions be made, it offers a rational framework for 1) accounting for systems in which unreacted solids and condensed phase products form a large fraction of the mass and volume of the total system, and 2) accounting for the transfer of mass, momentum, and energy both within and between phases. The methodology was illustrated by applying it to a device which is well characterized by experiments: the NSI driven pin puller.

*Presented at the Second NASA Aerospace Pyrotechnic Systems Workshop, February 8-9, 1994, Sandia National Laboratories, Albuquerque, New Mexico. This study is supported by the NASA Lewis Research Center under Contract Number NAG-1335. Dr. Robert M. Stubbs is the contract monitor.

†Graduate Research Assistant.

‡Assistant Professor, corresponding author.

The focus of this paper is on using the methodology presented in Ref. 5 to formulate a pin puller model which additionally accounts for the flow of combustion products through an orifice located within the device; the model is then used to determine the influence of product mass flow rates on the performance of the device. The present model also accounts for multiple pyrotechnic grains and variable burn surface area. The model presented in this paper is an extension of the model presented in Ref. 5 which did not account for product flow through the orifice, multiple grains, or variable burn surface area.

Figure 1 depicts a cross-section of the NSI driven pin puller in its unretracted state.[6] The primary pin, which will be referred to as the pin for the remainder of the paper, is driven by gases generated by the combustion of a pyrotechnic which is contained within the NSI assembly. Two NSI's are tightly threaded into the device's main body. Only one NSI need operate for the proper functioning of the pin puller; the second is a safety precaution in the event of failure of the first. The pyrotechnic consists of a 114 mg mixture of zirconium fuel (54.7 mg Zr) and potassium perchlorate oxidizer (59.3 mg $KClO_4$). Initially a thin diaphragm tightly encloses the pyrotechnic. Combustion is initiated by the transfer of heat from an electric bridgewire to the pyrotechnic. Upon ignition, the pyrotechnic undergoes rapid chemical reaction producing both condensed phase and gas phase products. The high pressure products accelerate the combustion rate, burst the confining diaphragm, vent through the NSI port (labeled "port" in Fig. 1), and enter into the gas expansion chamber. Once in the chamber, the high pressure gas first causes a set of shear pins to fail, then pushes the pin. After the pin is stopped by crushing an energy absorbing cup, the operation of the device is complete. Peak pressures within the expansion chamber are typically around 50.0 MPa; completion of the stroke requires approximately 0.5 ms.[6]

For sufficiently high NSI assembly/gas expansion chamber pressure ratios (~ 2.0), and for a fixed cross-sectional area of the NSI port, there exists a maximum flow rate of combustion product mass through the port. The occurrence of this maximum flow rate is referred to as a choked flow condition. Such a condition results in the maximum flux of energy into the expansion chamber; the energy contained within the chamber can then be used to perform work in moving the pin and can be lost to the surroundings in the form of heat. However, if the time scales associated with the flux of energy into the expansion chamber and the rate of heat lost from the products within the chamber to the surroundings are of the same magnitude, there may be insufficient energy available to move the pin; functional failure of the device would result. Therefore, it is possible that variations in the flow rate of product mass through the port may significantly affect the performance of the device.

Included in this report are 1) a description of the model including both the formulation of the model in terms of the mass, momentum, and energy principles supplemented by geometrical and constitutive relations and the mathematical reductions used to refine the model into a form suitable for numerical computations, 2) model predictions and comparisons with experimental results, and 3) results showing the sensitivity of the model to changes in the cross-sectional area of the NSI port.

Model Description

Assumptions for the model are as follows. As depicted in Fig. 2, the total system is taken to consist of three subsystems: incompressible solid pyrotechnic reactants (s), incompressible condensed phase products (cp), and gas phase products (g). The solid pyrotechnic is assumed to consist of N spherical grains having uniform instantaneous radii. The surroundings are taken to consist of the walls of the NSI assembly, the NSI port, and

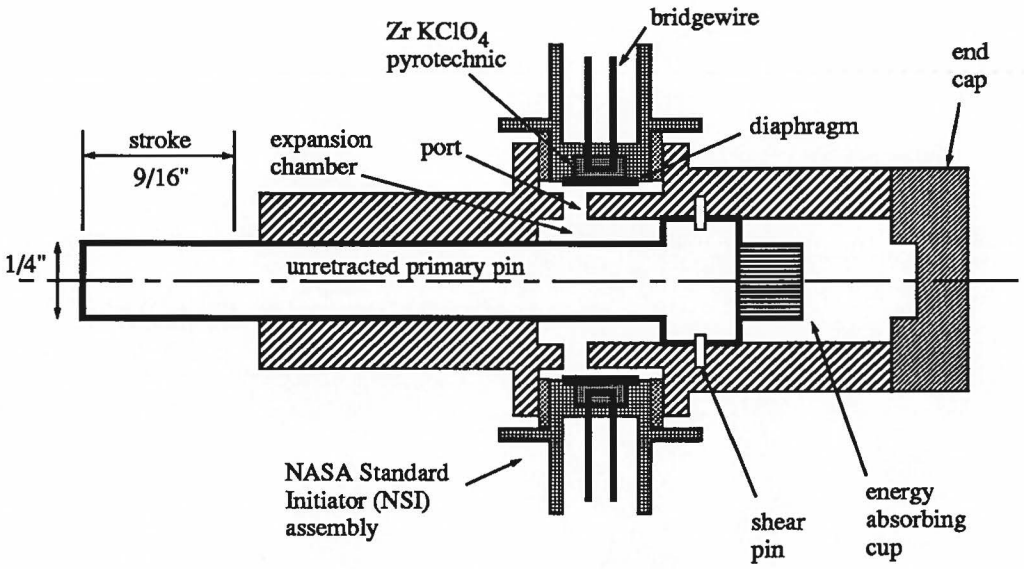

Figure 1: Cross-sectional view of the NSI driven pin puller.

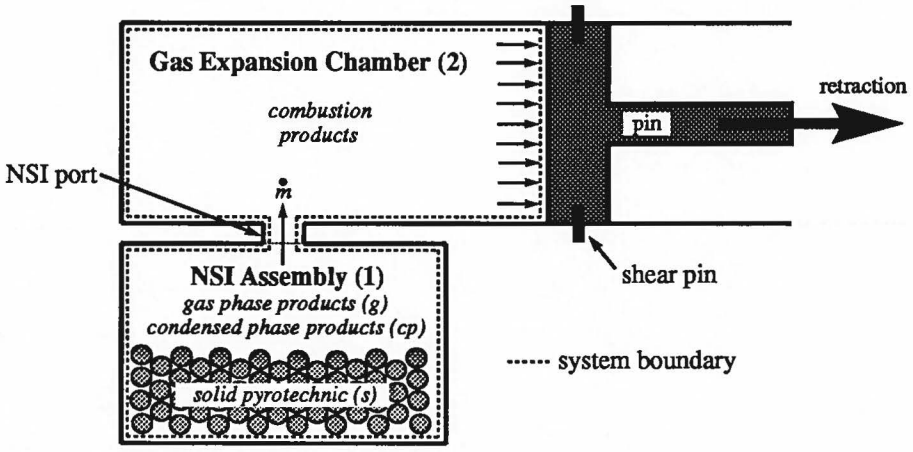

Figure 2: Schematic of the two component system for modeling choked flow effects.

the gas expansion chamber. Both the NSI assembly and the gas expansion chamber are modeled as isothermal cylindrical vessels. The gas expansion chamber is bounded at one end by a movable, frictionless, adiabatic pin while the volume of the NSI assembly remains constant for all time. The NSI port is assumed to have zero volume and is characterized by its cross-sectional area.

Mass and heat exchange between subsystems is allowed such that 1) mass can be transferred from the solid pyrotechnic to both the condensed phase and gas phase products, and 2) heat can be transferred from the condensed phase to the gas phase products. The condensed phase - gas phase heat transfer rate is assumed to be sufficiently large such that thermal equilibrium between the product subsystems exists. There is no mass exchange between the system and the surroundings. Both product subsystems are allowed to interact across the system boundary in the form of heat exchanges. The gas phase products are allowed to do expansion work on the surroundings. No work exchange between subsystems is

allowed. Spatial variations within subsystems are neglected; consequently, all variables are only time-dependent and the total system is modeled as a well-stirred reactor. The kinetic energy of the subsystems is ignored, while an accounting is made of the kinetic energy of the bounding pin. Body forces are neglected.

The rate of mass exchange from the reactant subsystem to the product subsystems is taken to be related to the gas phase pressure within the NSI assembly, namely $dr/dt = -bP_{g_1}^n$, where r is the instantaneous radii of the pyrotechnic grains, t is time, P_{g_1} is the gas phase pressure within the NSI assembly, and b and n are experimentally determined constants. All combustion is restricted to the burn surface of the pyrotechnic grains. In the absence of burn rate data for $Zr/KClO_4$, we have chosen values for b and n so that pressure-time predictions of our model agree with experimental data. The equilibrium thermochemistry code CET89[7] calculated for the constant volume complete combustion of the $Zr/KClO_4$ mixture is used to predict the product composition; the initial total volume of the pin puller ($0.95\ cm^3$) was used in this calculation since a significant portion of the system mass is contained within the gas expansion chamber at the time of complete combustion. The component gases are taken to be ideal with temperature-dependent specific heats. The specific heats are in the form of fourth-order polynomial curve fits given by the CET89 code and are not repeated here.

The rate of gas phase product mass flowing from the NSI assembly, through the NSI port, and into the gas expansion chamber is modeled using standard principles of gas dynamics. The flow of condensed phase product mass through the port is assumed to be proportional to the gas phase mass flow rate. The only energy interaction between the NSI assembly and the gas expansion chamber is due to the energy flux associated with the exchange of mass between these two components.

Using principles of mixture theory, a set of mass and energy evolution equations can be written for each subsystem contained within the NSI assembly and gas expansion chamber. These equations, coupled with an equation of motion for the pin, form a set of ordinary differential equations (ODE's) given by the following:

$$\frac{d}{dt}\left(\rho_{s_1} V_{s_1}\right) = -\rho_{s_1} A_b r_b, \tag{1}$$

$$\frac{d}{dt}\left(\rho_{cp_1} V_{cp_1}\right) = \eta_{cp} \rho_{s_1} A_b r_b - \dot{m}_{cp}, \tag{2}$$

$$\frac{d}{dt}\left(\rho_{g_1} V_{g_1}\right) = \left(1 - \eta_{cp}\right) \rho_{s_1} A_b r_b - \dot{m}_g, \tag{3}$$

$$\frac{d}{dt}\left(\rho_{s_1} V_{s_1} e_{s_1}\right) = -\rho_{s_1} e_{s_1} A_b r_b, \tag{4}$$

$$\frac{d}{dt}\left(\rho_{cp_1} V_{cp_1} e_{cp_1}\right) = \eta_{cp} \rho_{s_1} e_{s_1} A_b r_b - h_{cp_1} \dot{m}_{cp} - \dot{Q}_{cp,g_1} + \dot{Q}_{cp_1}, \tag{5}$$

$$\frac{d}{dt}\left(\rho_{g_1} V_{g_1} e_{g_1}\right) = \left(1 - \eta_{cp}\right) \rho_{s_1} e_{s_1} A_b r_b - h_{g_1} \dot{m}_g + \dot{Q}_{cp,g_1} + \dot{Q}_{g_1}, \tag{6}$$

$$\frac{d}{dt}\left(\rho_{cp_2} V_{cp_2}\right) = \dot{m}_{cp}, \tag{7}$$

$$\frac{d}{dt}\left(\rho_{g_2} V_{g_2}\right) = \dot{m}_g, \tag{8}$$

$$\frac{d}{dt}\left(\rho_{cp_2} V_{cp_2} e_{cp_2}\right) = h_{cp_1} \dot{m}_{cp} - \dot{Q}_{cp,g_2} + \dot{Q}_{cp_2}, \tag{9}$$

$$\frac{d}{dt}\left(\rho_{g_2} V_{g_2} e_{g_2}\right) = h_{g_1}\dot{m}_g + \dot{Q}_{cp,g_2} + \dot{Q}_{g_2} - \dot{W}_{out_2}, \tag{10}$$

$$m_p \frac{d^2}{dt^2}\left(z_p\right) = F_p. \tag{11}$$

In these equations, the notation subscript "1" and subscript "2" are used to label quantities associated with the NSI and the gas expansion chamber, respectively. Subscripts "s", "cp", and "g" are used to label quantities associated with the solid pyrotechnic, condensed phase products, and gas phase products, respectively. The independent variable in Eqs. (1-11) is time t. Dependent variables are as follows: the density ρ_{g_i} (here, and for the remainder of this report, the index $i = 1, 2$ will be used to denote quantities associated with the NSI and the gas expansion chamber, respectively); the volumes V_{s_1}, V_{cp_i}, V_{g_i}; the specific internal energies e_{s_1}, e_{cp_i}, e_{g_i}; the specific enthalpies h_{cp_1}, h_{g_1}; the pin position z_p; the pyrotechnic burn rate r_b; the area of the burn surface A_b; the rates of product mass flowing through the NSI port $\dot{m}_{cp}$, $\dot{m}_g$; the rates of heat transfer from the surroundings to the gas phase products $\dot{Q}_{in_i}$; the rates of heat transfer from the condensed phase products to the gas phase products $\dot{Q}_{cp,g_i}$; the rate of work done by product gases contained within the expansion chamber in moving the pin $\dot{W}_{out_2}$; and the net force on the pin F_p.

Constant parameters contained in Eqs. (1-11) are the mass of the pin m_p, the density of the unreacted solid pyrotechnic ρ_{s_1}, the density of the condensed phase products ρ_{cp_1} and ρ_{cp_2}, and the mass fraction of the products which are in the condensed phase η_{cp}. As it is understood that the pyrotechnic is contained entirely within the NSI, the notation subscript "1" will be dropped when referring to quantities associated with the solid pyrotechnic. Also, since $\rho_{cp_1} = \rho_{cp_2} =$ constant, these two quantities will be referred to as ρ_{cp}.

Equations (1-3) govern the evolution of mass and Eqs. (4-6) govern the evolution of energy for the solid pyrotechnic, the condensed phase products, and the gas phase products contained within the NSI, respectively. Equations (7) and (8) govern the evolution of mass and Eqs. (9) and (10) govern the evolution of energy for the condensed phase products and gas phase products contained within the gas expansion chamber, respectively. Equation (11) is Newton's Second Law which governs the motion of the pin.

Geometric and constitutive relations used to close Eqs. (1-11) are as follows:

$$V_1 = V_s + V_{cp_1} + V_{g_1}, \tag{12}$$

$$V_2 = V_{cp_2} + V_{g_2}, \tag{13}$$

$$z_p = \frac{V_2}{A_p}, \tag{14}$$

$$r\left[V_s\right] = \left(\frac{3V_s}{4\pi N}\right)^{1/3}, \tag{15}$$

$$A_b\left[V_s\right] = \left(36\pi N V_s^2\right)^{1/3}, \tag{16}$$

$$P_{g_i} = \rho_{g_i} R T_{g_i}, \tag{17}$$

$$r_b\left[P_{g_1}\right] = -\frac{dr}{dt} = b P_{g_1}^n, \tag{18}$$

$$e_s\left[T_s\right] = \sum_{j=1}^{N_s} Y_s^j e_s^j\left[T_s\right], \tag{19}$$

$$e_{cp_i}\left[T_{cp_i}\right] = \sum_{j=1}^{N_{cp}} Y_{cp}^{j} e_{cp}^{j}\left[T_{cp_i}\right], \tag{20}$$

$$e_{g_i}\left[T_{g_i}\right] = \sum_{j=1}^{N_g} Y_g^j e_g^j\left[T_{g_i}\right], \tag{21}$$

$$c_{vs}\left[T_s\right] = \sum_{j=1}^{N_s} Y_s^j \frac{d}{dT_s}\left(e_s^j\left[T_s\right]\right), \tag{22}$$

$$c_{vcp_i}\left[T_{cp_i}\right] = \sum_{j=1}^{N_{cp}} Y_{cp}^{j} \frac{d}{dT_{cp_i}}\left(e_{cp}^{j}\left[T_{cp_i}\right]\right), \tag{23}$$

$$c_{vg_i}\left[T_{g_i}\right] = \sum_{j=1}^{N_g} Y_g^j \frac{d}{dT_{g_i}}\left(e_g^j\left[T_{g_i}\right]\right), \tag{24}$$

$$h_{cp_1}\left[T_{cp_1}\right] = \sum_{j=1}^{N_{cp}} Y_{cp}^{j} h_{cp}^{j}\left[T_{cp_1}\right], \tag{25}$$

$$h_{g_1}\left[T_{g_1}\right] = \sum_{j=1}^{N_g} Y_g^j h_g^j\left[T_{g_1}\right], \tag{26}$$

$$c_{pcp_1}\left[T_{cp_1}\right] = \sum_{j=1}^{N_{cp}} Y_{cp}^{j} \frac{d}{dT_{cp_1}}\left(h_{cp}^{j}\left[T_{cp_1}\right]\right), \tag{27}$$

$$c_{pg_1}\left[T_{g_1}\right] = \sum_{j=1}^{N_g} Y_g^j \frac{d}{dT_{g_1}}\left(h_g^j\left[T_{g_1}\right]\right), \tag{28}$$

$$\dot{Q}_{cp,g_i}\left[T_{cp_i}, T_{g_i}\right] = h_{cp,g} A_{cp_i}\left(T_{cp_i} - T_{g_i}\right), \tag{29}$$

$$\dot{Q}_{cp_i} = \dot{Q}_{cp_i}\left[T_{cp_i}\right], \tag{30}$$

$$\dot{Q}_{g_i} = \dot{Q}_{g_i}\left[T_{g_i}\right], \tag{31}$$

$$\dot{W}_{out_2} = P_{g_2} \frac{dV_2}{dt}, \tag{32}$$

$$F_p = \begin{cases} 0 & \text{if } P_{g_2} A_p < F_{crit} \\ P_{g_2} A_p & \text{if } P_{g_2} A_p \geq F_{crit}, \end{cases} \tag{33}$$

$$\dot{m}_g = \begin{cases} \rho_{g_1} A_e \sqrt{\gamma R T_{g_1}} \sqrt{\frac{2}{\gamma-1}\left(\frac{P_{g_1}}{P_{g_2}}\right)^{-\frac{\gamma+1}{\gamma}}\left(\left(\frac{P_{g_1}}{P_{g_2}}\right)^{\frac{\gamma-1}{\gamma}} - 1\right)} & \text{if } \left(\frac{P_{g_1}}{P_{g_2}}\right) < \left(\frac{\gamma+1}{2}\right)^{\frac{\gamma}{\gamma-1}} \\ \rho_{g_1} A_e \sqrt{\gamma R T_{g_1}} \left(\frac{2}{\gamma+1}\right)^{\frac{\gamma+1}{2(\gamma-1)}} & \text{if } \left(\frac{P_{g_1}}{P_{g_2}}\right) \geq \left(\frac{\gamma+1}{2}\right)^{\frac{\gamma}{\gamma-1}}, \end{cases} \tag{34}$$

$$\dot{m}_{cp} = \left(\frac{\eta_{cp}}{1-\eta_{cp}}\right) \dot{m}_g. \tag{35}$$

Here, and throughout the paper, braces [ ] are used to denote a functional dependence on the enclosed variable. Equations (12-14) are geometrical constraints; in Eq. (14), A_p is the cross-sectional area of the pin. Equation (15) is an expression for the radius r of each

spherical pyrotechnic grain; N is the total number of pyrotechnic grains. The area of the burn surface is given by Eq. (16); it is assumed here that the area of the burning surface is the total surface area of the N pyrotechnic grains. Equation (17) is a thermal equation of state for the gas phase products. Occurring in this expression are the gas phase pressure P_{g_i}, the gas phase temperature T_{g_i}, and the ideal gas constant for the gas phase products R (the quotient of the universal gas constant and the mean molecular weight of the product gases). The pyrotechnic burn rate r_b is given by Eq. (18).

Equations (19-21) are caloric equations of state for the solid pyrotechnic, condensed phase products, and gas phase products, respectively. Here, T_s is the temperature of the solid pyrotechnic, and T_{cp_i} is the temperature of the condensed phase products. Also, Y_s^j, $Y_{cp_i}^j$, $Y_{g_i}^j$, N_s, N_{cp}, and N_g are the constant mass fractions and number of component species of solid pyrotechnic, condensed phase product, and gas phase product species, respectively. Here, and throughout the paper, the notation superscript "j" is used to label quantities associated with individual chemical species. Since for both ideal gases and condensed phase species, the internal energy is only a function of temperature, the specific heat at constant volume for the solid pyrotechnic, c_{vs}, the condensed phase products, c_{vcp_i}, and the gas phase products, c_{vg_i}, can be obtained by differentiation of Eqs. (19-21) with respect to their temperature. Expressions for the specific heats at constant volume are given by Eqs. (22-24). The specific enthalpies for the condensed phase products and the gas phase products contained within the NSI assembly are given by Eqs. (25) and (26), respectively. These expressions can be differentiated with respect to their temperature to obtain the specific heats at constant pressure c_{pcp_1} and c_{pg_1}, Eqs. (27) and (28).

Equation (29) gives an expression for the rate of heat transfer from the condensed phase products to the gas phase products. In this expression, $h_{cp,g}$ is a constant heat transfer parameter, and A_{cp_i} is the surface area of the condensed phase products. The term $h_{cp,g}A_{cp_i}$ is assumed large for this study. The functional dependencies of the heat transfer rates between the surroundings and the product subsystems are given by Eqs. (30) and (31). The functional form of these models will be given below.

Equation (32) models pressure-volume work done by the gas contained within the expansion chamber in moving the pin. Equation (33) models the force on the pin due to the gas phase pressure and a restraining force due to the shear pins which are used to initially hold the pin in place. Here, F_{crit} is the critical force necessary to cause shear pin failure. The work associated with shearing the pin is not considered.

The flow rate of gas phase product mass through the NSI port is given by Eq. (34).[8] Occurring in this expression are the cross-sectional area of the port, A_e, and the specific heat ratio for the product gases contained within the NSI assembly, γ $(= c_{pg_1}/c_{vg_1})$. This expression accounts for mass choking at elevated NSI assembly/gas expansion chamber pressure ratios. The condensed phase product mass flow rate through the port is given by Eq. (35).

With the assumption of large heat transfer rates between the condensed phase and gas phase product subsystems (*i.e.*, $h_{cp,g}A_{cp_i} \to \infty$), the product subsystems remain in thermal equilibrium for all time. Therefore, we take $T_{p_1} \equiv T_{cp_1} = T_{g_1}$ and $T_{p_2} \equiv T_{cp_2} = T_{g_2}$, with T_{p_1} defined as the temperature of the combined product subsystem contained within the NSI assembly and T_{p_2} the temperature of the combined product subsystem contained within the gas expansion chamber. With this assumption, one can define the net heat transfer rates $\dot{Q}_{p_1}$ and $\dot{Q}_{p_2}$ governing the transfer of heat from the surroundings to the combined product

subsystems:

$$\dot{Q}_{p_1}[T_{p_1}] \equiv \dot{Q}_{cp_1} + \dot{Q}_{g_1} = hA_{w_1}(T_w - T_{p_1}) + \sigma A_{w_1}\left(\alpha T_w^4 - \epsilon T_{p_1}^4\right), \tag{36}$$

$$\dot{Q}_{p_2}[T_{p_2}] \equiv \dot{Q}_{cp_2} + \dot{Q}_{g_2} = hA_{w_2}[V_s](T_w - T_{p_2}) + \sigma A_{w_2}[V_2]\left(\alpha T_w^4 - \epsilon T_{p_2}^4\right), \tag{37}$$

where

$$A_{w_1} = 2\sqrt{\frac{\pi}{A_1}}V_1 + 2A_1 - A_e, \qquad A_{w_2}[V_2] = 2\sqrt{\frac{\pi}{A_p}}V_2 + A_p - A_e. \tag{38}$$

Equations (38) are expressions for the surface area of the NSI assembly and the gas expansion chamber, respectively, through which heat transfer with the surroundings can occur; the parameter A_1 in the first of these relations is the constant cross-sectional area of the NSI assembly.

Mathematical Reductions

In this section, intermediate operations are described that reduce the governing equations to a final autonomous system of first order ODE's which can be numerically solved to predict the pin puller performance. To this end, it is necessary to define a new variable $\dot{V}_2$ representing the time derivative of the gas expansion chamber volume:

$$\dot{V}_2 \equiv \frac{dV_2}{dt}. \tag{39}$$

The final system consists of eight first order ODE's of the form

$$\frac{d\mathbf{u}}{dt} = \mathbf{f}(\mathbf{u}), \tag{40}$$

where $\mathbf{u} = (V_2, V_s, V_{cp_1}, \rho_{g_1}, T_{p_1}, V_{cp_2}, T_{p_2}, \dot{V}_2)^T$ is a vector of dependent variables and $\mathbf{f}$ is a non-linear vector function. These eight dependent variables will be referred to as primary variables. It will now be shown how to express all remaining variables as functions of the primary variables.

Quantities already expressed in terms of the primary variables are the gas phase pressure inside the NSI $P_{g_1}[\rho_{g_1}, T_{p_1}]$, the heat transfer rates $\dot{Q}_{p_1}[T_{p_1}]$ and $\dot{Q}_{p_2}[V_2, T_{p_2}]$, the specific internal energies $e_{cp_i}[T_{p_i}]$ and $e_{g_i}[T_{p_i}]$, the specific heats at constant volume $c_{vcp_i}[T_{p_i}]$ and $c_{vg_i}[T_{p_i}]$, the specific enthalpies $h_{cp_1}[T_{p_1}]$ and $h_{g_1}[T_{p_1}]$, and the specific heats at constant pressure $c_{pcp_1}[T_{p_1}]$ and $c_{pg_1}[T_{p_1}]$. Also, with a knowledge of P_{g_1}, Eq. (18) can be used to express r_b as functions of ρ_{g_1} and T_{p_1}:

$$r_b[\rho_{g_1}, T_{p_1}] = bP_{g_1}^n[\rho_{g_1}, T_{p_1}]. \tag{41}$$

Addition of Eqs. (1), (2), (3), (7), and (8) results in a homogeneous differential equation expressing the conservation of the total system's mass:

$$\frac{d}{dt}(\rho_s V_s + \rho_{cp}V_{cp_1} + \rho_{g_1}V_{g_1} + \rho_{cp}V_{cp_2} + \rho_{g_2}V_{g_2}) = 0. \tag{42}$$

Integrating this expression, applying initial conditions, denoted by the subscript "o", using Eq. (12) to eliminate V_{g_1} in favor of V_1, V_s, and V_{cp_1}, using Eq. (13) to eliminate V_{g_2} in favor of V_2 and V_{cp_2}, and solving for ρ_{g_2} results in the following:

$$\rho_{g_2}[V_2, V_s, V_{cp_1}, \rho_{g_1}, V_{cp_2}] = \frac{m_o - \rho_s V_s - \rho_{cp}V_{cp_1} - \rho_{g_1}(V_1 - V_s - V_{cp_1}) - \rho_{cp}V_{cp_2}}{V_2 - V_{cp_2}}, \tag{43}$$

where

$$m_o = \rho_s V_{s_o} + \rho_{cp} V_{cp_1 o} + \rho_{g_1 o} V_{g_1 o} + \rho_{cp} V_{cp_2 o} + \rho_{g_2 o} V_{g_2 o}.$$

Here, m_o represents the initial mass of the system. Substituting Eq. (43) into Eq. (17) determines P_{g_2} as a function of the primary variables:

$$P_{g_2}\left[V_2, V_s, V_{cp_1}, \rho_{g_1}, V_{cp_2}, T_{p_2}\right] = \rho_{g_2}\left[V_2, V_s, V_{cp_1}, \rho_{g_1}, V_{cp_2}\right] R T_{p_2}. \tag{44}$$

With a knowledge of P_{g_2}, Eqs. (32), (33), (34), and (35) can be expressed in the following forms, respectively:

$$\dot{W}_{out2} = \dot{W}_{out2}[V_2, V_s, V_{cp_1}, \rho_{g_1}, V_{cp_2}, T_{p_2}, \dot{V}_2], \tag{45}$$

$$F_p = F_p\left[V_2, V_s, V_{cp_1}, \rho_{g_1}, V_{cp_2}, T_{p_2}\right], \tag{46}$$

$$\dot{m}_g = \dot{m}_g\left[V_2, V_s, V_{cp_1}, \rho_{g_1}, T_{p_1}, V_{cp_2}, T_{p_2}\right], \tag{47}$$

$$\dot{m}_{cp} = \dot{m}_{cp}\left[V_2, V_s, V_{cp_1}, \rho_{g_1}, T_{p_1}, V_{cp_2}, T_{p_2}\right]. \tag{48}$$

We next simplify the remaining mass evolution equations. Since both ρ_s and ρ_{cp} are constant, Eqs. (1), (2), and (7) can be rewritten as

$$\frac{dV_s}{dt} = -A_b r_b, \tag{49}$$

$$\frac{dV_{cp_1}}{dt} = \frac{\eta_{cp}\rho_s A_b r_b - \dot{m}_{cp}}{\rho_{cp}}, \tag{50}$$

$$\frac{dV_{cp_2}}{dt} = \frac{\dot{m}_{cp}}{\rho_{cp}}. \tag{51}$$

To simplify Eq. (3), we use Eq. (12) to replace V_{g_1} in favor of V_s and V_{cp_1}, use Eqs. (49) and (50) to eliminate the resulting volume derivatives, and solve for the time derivative of ρ_{g_1}:

$$\frac{d\rho_{g_1}}{dt} = \frac{\left(1 - \frac{\rho_{g_1}}{\rho_s} - \left(1 - \frac{\rho_{g_1}}{\rho_{cp}}\right)\eta_{cp}\right)\rho_s A_b r - \dot{m}_g - \frac{\rho_{g_1}}{\rho_{cp}}\dot{m}_{cp}}{V_1 - V_s - V_{cp_1}}. \tag{52}$$

The energy evolution equations will now be simplified. We first multiply Eq. (1) by e_s and subtract the result from Eq. (4) to obtain

$$\frac{de_s}{dt} = 0.$$

Thus, in accordance with our assumption of no heat transfer to the solid pyrotechnic, its specific internal energy remains constant for all time. Integrating this result, we obtain

$$e_s = e_{s_o}. \tag{53}$$

Addition of Eqs. (5) and (6), and addition of Eqs. (9) and (10) result in expressions governing the evolution of energy for the combined product subsystems contained within the NSI assembly and gas expansion chamber, respectively:

$$\frac{d}{dt}\left[\rho_{cp} V_{cp_1} e_{cp_1} + \rho_{g_1} V_{g_1} e_{g_1}\right] = \rho_s e_s A_b r_b - h_{cp_1}\dot{m}_{cp} - h_{g_1}\dot{m}_g + \dot{Q}_{p_1}, \tag{54}$$

$$\frac{d}{dt}\left[\rho_{cp}V_{cp_2}e_{cp_2} + \rho_{g_2}V_{g_2}e_{g_2}\right] = h_{cp_1}\dot{m}_{cp} + h_{g_1}\dot{m}_g + \dot{Q}_{p_2} - \dot{W}_{out_2}. \tag{55}$$

The net heat transfer rates given by Eqs. (36) and (37) have been incorporated into these expressions. Multiplying Eq. (2) by e_{cp_1}, multiplying Eq. (3) by e_{g_1}, subtracting these results from Eq. (54), using Eqs. (20) and (21) to re-express the derivatives in terms of T_{p_1}, and solving for the derivative of T_{p_1} yields:

$$\frac{dT_{p_1}}{dt} = \frac{\rho_s\left(e_s - \eta_{cp}e_{cp_1} - (1-\eta_{cp})\,e_{g_1}\right)A_b r_b - \left(h_{cp_1} - e_{cp_1}\right)\dot{m}_{cp} - \left(h_{g_1} - e_{g_1}\right)\dot{m}_g + \dot{Q}_{p_1}}{\rho_{cp}V_{cp_1}c_{vcp_1} + \rho_{g_1}V_{g_1}c_{vg_1}}. \tag{56}$$

Similarly, multiplying Eq. (7) by e_{cp_2}, multiplying Eq. (8) by e_{g_2}, subtracting these results from Eq. (55), using Eqs. (20) and (21) to re-express the derivatives in terms of T_{p_2}, and solving for the derivative of T_{p_2} yields:

$$\frac{dT_{p_2}}{dt} = \frac{\left(h_{cp_1} - e_{cp_2}\right)\dot{m}_{cp} + \left(h_{g_1} - e_{g_2}\right)\dot{m}_g + \dot{Q}_{p_2} - \dot{W}_{out_2}}{\rho_{cp}V_{cp_2}e_{cp_2}c_{vcp_2} + \rho_{g_2}V_{g_2}c_{vg_2}}. \tag{57}$$

Lastly, Eq. (11) can be split into two first order ODE's. The first of these equations is given by the definition presented in Eq. (39). The second equation, obtained by using Eq. (39) and the geometrical relation given by Eq. (14), is expressed by the following:

$$\frac{d\dot{V}_2}{dt} = \frac{A_p F_p}{m_p}. \tag{58}$$

Equation (39), (49), (50), (52), (56), (51), (57), and (58) for a coupled set of eight non-linear first order ODE's in eight unknowns. Initial conditions for these equations are

$$\begin{array}{lll} V_2(t=0) = V_{2o}, & V_s(t=0) = V_{so}, & V_{cp_1}(t=0) = V_{cp_1o}, \\ \rho_{g_1}(t=0) = \rho_{g_1o}, & T_{p_1}(t=0) = T_o, & V_{cp_2}(t=0) = V_{cp_2o}, \\ T_{p_2}(t=0) = T_o, & \dot{V}_2(t=0) = 0. & \end{array} \tag{59}$$

All other quantities of interest can be obtained once these equations are solved.

Results

Numerical solutions were obtained for the simulated firing of an NSI into the pin puller device. The numerical algorithm used to perform the integrations was a stiff ODE solver given in the standard code LSODE. The combustion process predicted by the CET89 chemical equilibrium code followed the chemical equation given in Table 1. Parameters used in the simulations are given in Table 2.

Predictions for the pressure history inside the NSI and the gas expansion chamber are shown in Fig. 3. Also shown in this figure are experimental values obtained by pressure transducers located inside the gas expansion chamber.[9] A rapid increase in pressure is predicted within the NSI assembly immediately following combustion initiation ($t = 0$ ms); the pressure continually rises to a maximum value near 195 MPa occurring near the time of complete combustion ($t = 0.023$ ms). The pressure within the expansion chamber increases more slowly due to mass choking at the NSI port. Following completion of the combustion process, the pressure within the NSI assembly decreases to 53.9 MPa occurring near $t = 0.06$ ms; during this same time, the pressure within the gas expansion chamber uniformly increases to a maximum value of 53.4 MPa. There is a subsequent decrease in

both pressures to values near 22.5 MPa at completion of the pin's stroke ($t_{st} = 0.466\ ms$). These decreases in pressure result from work done by the product gases in moving the pin and heat transfer from the combined product subsystems to the surroundings.

Figure 4 shows the predicted temperature history for the combustion products contained within the NSI assembly and the gas expansion chamber. Since the only energy exchange between subsystems contained within these two components is due to the flux of product mass through the NSI port, the resulting temperatures of the combined product subsystems do not thermally equilibrate. Figure 5 shows the predicted density history for the gas phase products inside the NSI and the gas expansion chamber. As a consequence of the product temperature difference, a significant difference in gas phase density is also predicted.

The predicted velocity history of the combustion products flowing through the NSI port is given in Fig. 6. Here, a rapid rise in velocity to a maximum value near 928 m/s is predicted immediately following combustion initiation; during this time, the flow through the port becomes choked. The flow remains choked as the velocity slowly decreases to 830.3 m/s. Subsequently, there is a rapid decrease in velocity to a minimum value of approximately 7 m/s ocurring at $t = 0.63\ ms$. This rapid decrease in velocity occurs as the pressures within the NSI assembly and the gas expansion chamber equilibrate following completion of the combustion process. As the pin retracts, gases within the expansion chamber expand creating a slight pressure imbalance across the NSI port; consequently, the velocity of the flow begins to slowly increase to a value of 23 m/s at completion of the stroke.

Figure 7 shows the time history of the predicted pin kinetic energy. A continual increase in kinetic energy to a maximum value of approximately 31.4 J at completion of the stroke is predicted. This value compares to an experimentally measured value of approximately 22.6 J. The larger value for the predicted kinetic energy is consistent with the fact that frictional effects, which would tend to retard the motion of the pin, have not been accounted for in the model.

Figure 8 gives results showing the sensitivity of the model to changes in the NSI port cross-sectional area, A_e. For this study, we use the predicted pin puller solution as the baseline solution (baseline parameters given in Table 2). The sensitivity of the model is determined by solving the pin puller problem and finding the parametric dependency of three predicted quantities: the pin kinetic energy at completion of the stroke, the stroke time, and the maximum pressure attained within the NSI assembly. Quantities presented in this figure have been scaled by values obtained from the pin puller simulation presented above. For decreasing values of A_e, pin kinetic energy decreases while both the stroke time and maximum pressure within the NSI increase. These results are primarily due to smaller mass flow rates through the port resulting from decreasing port cross-sectional areas. For slightly larger values of A_e, both the stroke time and the pin kinetic energy approach a nearly constant value while the peak pressure within the NSI decreases.

Conclusions

The model presented in this paper is successful in predicting the dynamic events associated with the operation of an NSI driven pin puller. In addition to tracking the interactions between the reactant and product subsystems, the model also accounts for multiple pyrotechnic grains, variable burn surface area, and combustion product mass flow rates through the NSI port. Results of a sensitivity analysis reveal that variations in the cross-sectional area of the port may significantly effect the performance of the device. Specifically, significant decreases in the pin kinetic energy result from decreases in port cross-sectional

area. In the presence of friction, the smaller kinetic energy of the pin may be insufficient to overcome frictional effects resulting in functional failure. Decreases in cross-sectional area may arise from the partial blockage of the NSI port by foreign matter or by the accumulation of condensed phase combustion products. Moreover, it is possible that the very high predicted pressures within the NSI assembly resulting from decreasing port cross-sectional areas may be sufficient to cause structural failure of the NSI's webbing, thereby jamming the pin and preventing it from retracting. Such structural failures have been reported in the past.[6]

References

[1]Razani, A., Shahinpoor, M., and Hingorani-Norenberg, S. L., "A Semi-Analytical Model for the Pressure-Time History of Granular Pyrotechnic Materials in a Closed System," *Proceedings of the Fifteenth International Pyrotechnics Seminar*, Chicago, IL, 1990, pp. 799-813.

[2]Farren, R. E., Shortridge, R. G., and Webster, H. A., III, "Use of Chemical Equilibrium Calculations to Simulate the Combustion of Various Pyrotechnic Compositions," *Proceedings of the Eleventh International Pyrotechnics Seminar*, Vail, CO, 1986, pp. 13-40.

[3]Butler, P. B., Kang, J., and Krier, H., "Modeling of Pyrotechnic Combustion in an Automotive Airbag Inflator," *Proceedings - Europyro 93, 5^e Congrès International de Pyrotechnie du Groupe de Travaile de Pyrotechnie*, Strasbourg, France, 1993, pp. 61-70.

[4]Kuo, J. H., and Goldstein, S., "Dynamic Analysis of NASA Standard Initiator Driven Pin Puller," AIAA 93-2066, June 1993.

[5]Gonthier, K. A., and Powers, J. M., "Formulation, Predictions, and Sensitivity Analysis of a Pyrotechnically Actuated Pin Puller Model," *Journal of Propulsion and Power*, accepted for publication, 1993.

[6]Bement, L. J., Multhaup, H. A., and Schimmel, M. L., "HALOE Gimbal Pyrotechnic Pin Puller Failure Investigation, Redesign, and Qualification," NASA Langley Research Center, Report, Hampton, VA, 1991.

[7]Gordon, S., and McBride, B. J., "Computer Program for Calculation of Complex Chemical Equilibrium Compositions, Rocket Performance, Incident and Reflected Shocks, and Chapman-Jouguet Detonations," NASA Lewis Research Center, SP-273, Cleveland, OH, 1976.

[8]Fox, R. W., and McDonald, A. T., *Fundamentals of Heat and Mass Transfer*, 3rd ed. John Wiley and Sons, Inc. 1985, pp. 599-617.

[9]Bement, L. J., private communication, NASA Langley Research Center, Hampton, VA, 1992.

Table 1: Stoichiometric equation used in pin puller simulations.

$$
\begin{aligned}
4.0908Zr(s) + 2.9178KClO_4(s) \longrightarrow\ & 2.7198ZrO_2(cp) + 2.1786KCl(g) + 1.3310O(g) \\
& +1.2305ZrO_2(g) + 1.0136O_2(g) + 0.6472Cl(g) \\
& +0.4310K(g) + 0.2434KO(g) + 0.1403ZrO(g) \\
& +0.0288ClO(g) + 0.0285K_2Cl_2(g) + 0.0040K_2(g) \\
& +0.0031Cl_2(g) + 0.0002Zr(g) + 0.0001O_3(g).
\end{aligned}
$$

Table 2: Parameters used in pin puller simulation.

parameter	*value*
η_{cp}	0.43
N	100
A_e	0.100 cm^2
A_p	0.634 cm^2
A_1	0.634 cm^2
V_1	0.125 cm^3
ρ_s	3.57 g/cm^3
ρ_{cp}	5.89 g/cm^3
T_s	288.0 K
T_w	288.0 K
h	1.25×10^6 $g/s^3/K$
ϵ	0.60
α	0.60
F_{crit}	3.56×10^7 $dyne$
b	0.003 $(dyne/cm^2)^{-0.60} cm/s$
n	0.60
V_{2o}	0.824 cm^3
V_{so}	0.038 cm^3
V_{cp_1o}	7.425×10^{-8} cm^3
ρ_{g_1o}	6.202×10^{-6} g/cm^3
T_o	288.0 K
V_{cp_2o}	6.576×10^{-7} cm^3
V_2	0.0 cm^3/s

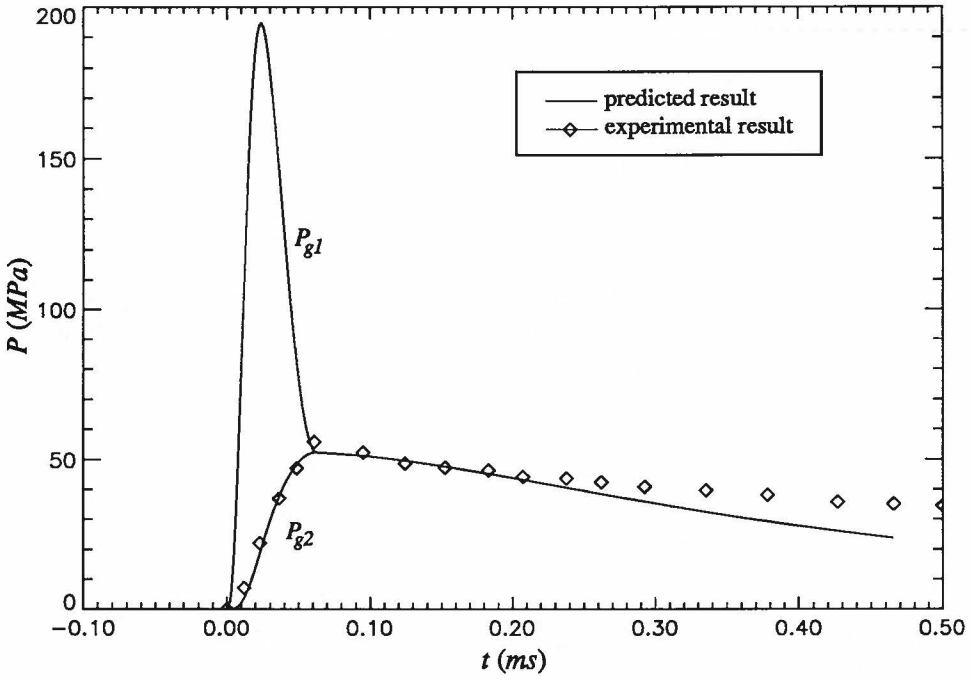

Figure 3: Predicted and experimental pressure histories for the pin puller simulation.

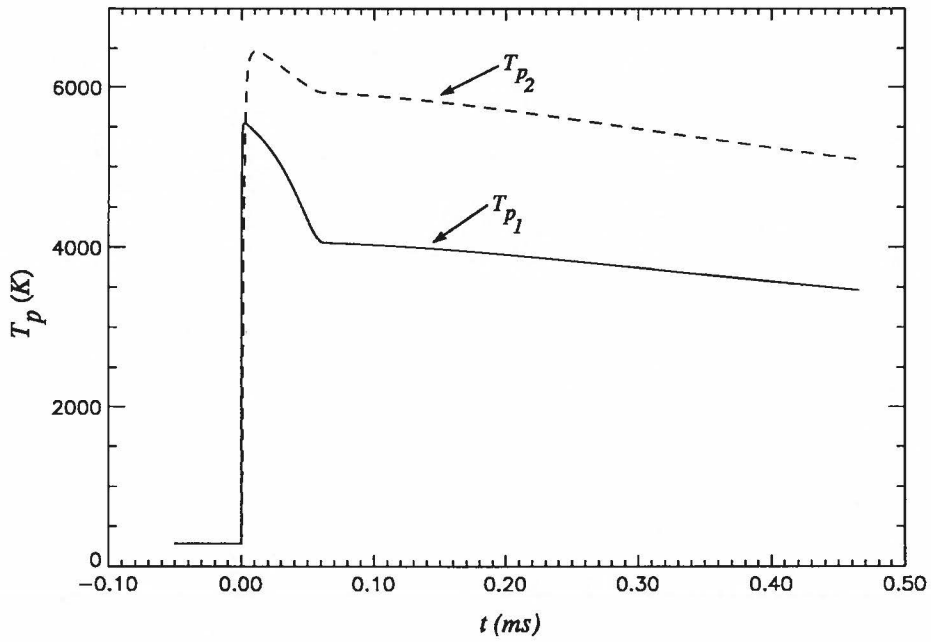

Figure 4: Predicted temperature histories for the pin puller simulation.

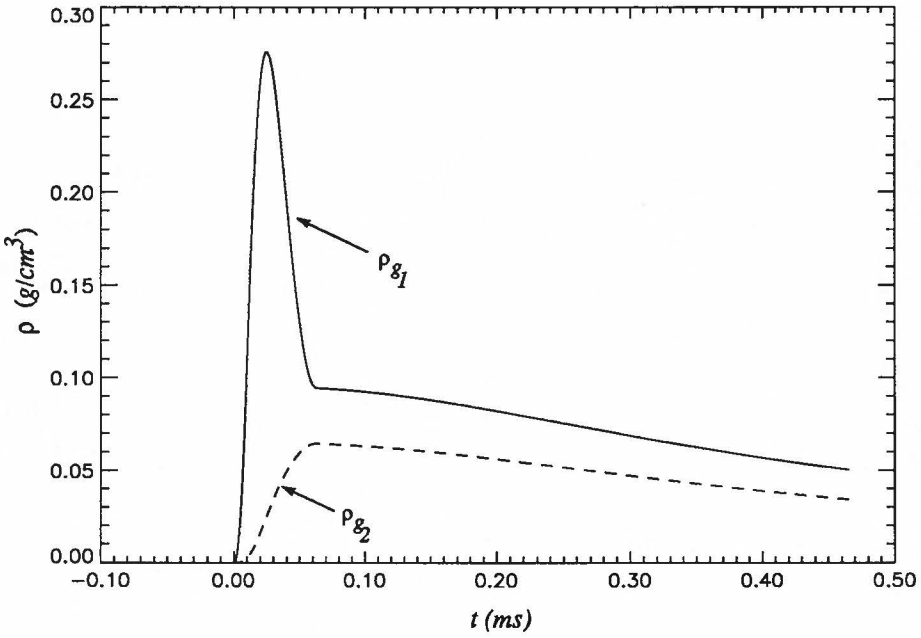

Figure 5: Predicted temperature histories for the pin puller simulation.

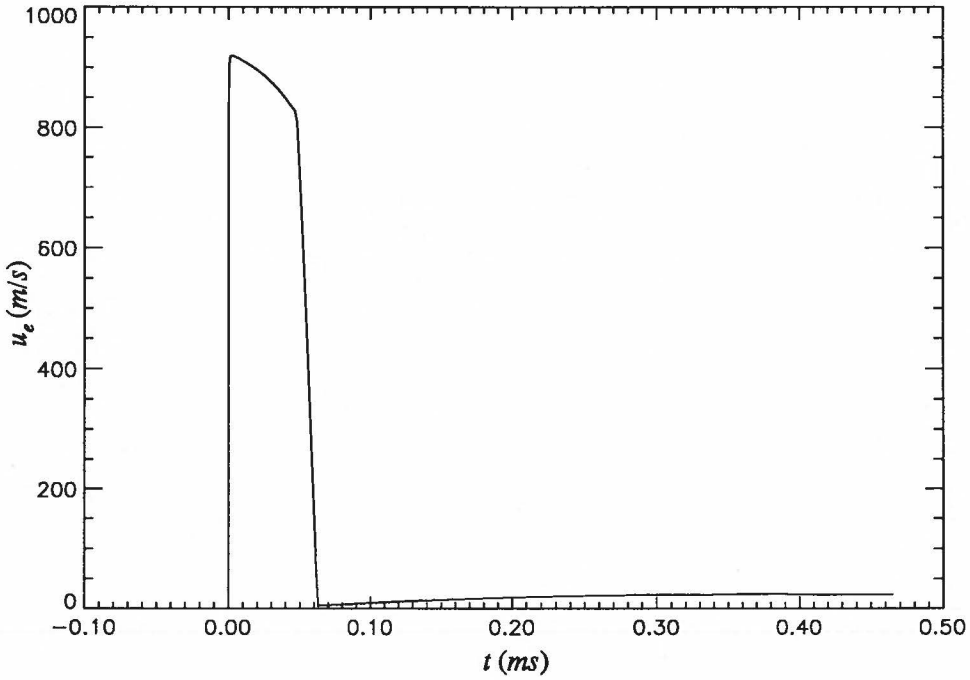

Figure 6: Predicted velocity of the flow through the NSI port for the pin puller simulation.

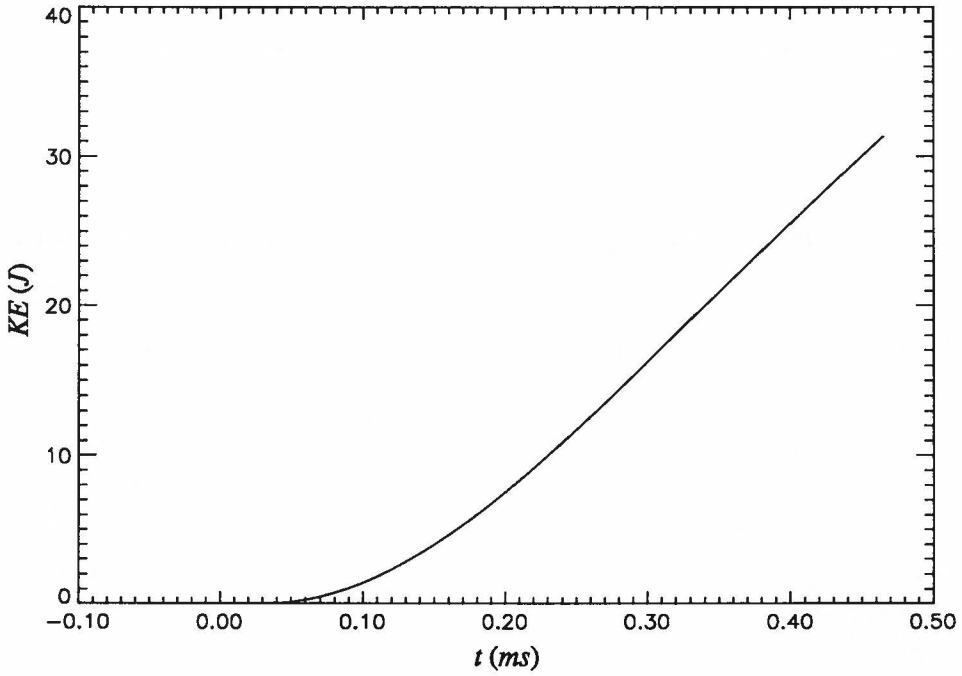

Figure 7: Predicted kinetic energy of the pin for the pin puller simulation.

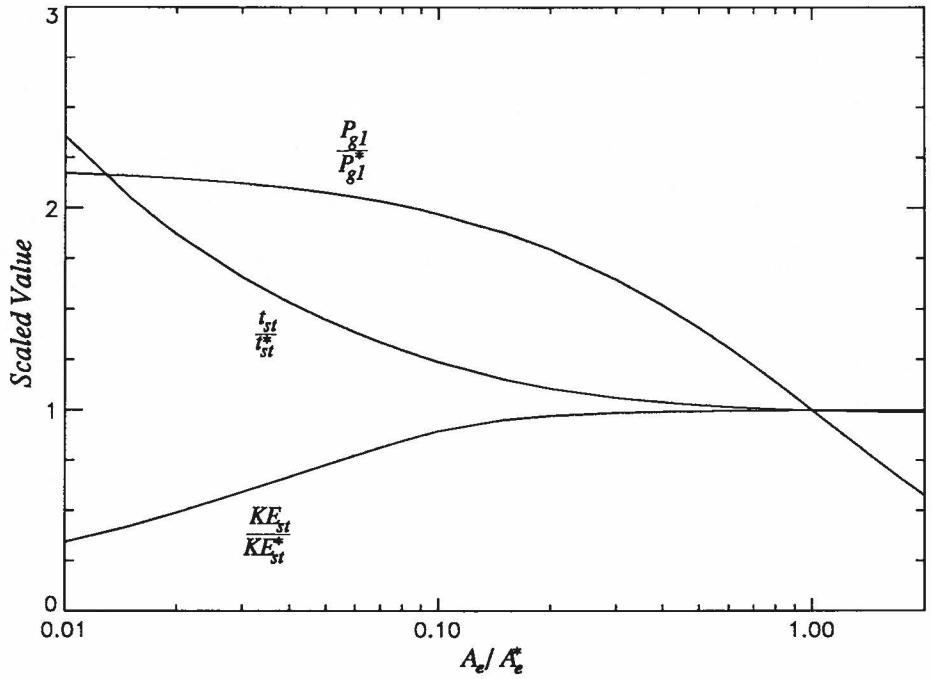

Figure 8: Sensitivity of the model to changes in the NSI port cross-sectional area. The values presented in this figure have been scaled by the gaseline values $A^*_e = 0.10\ cm^2$, $KE^* = 31.4\ J$, $t^*_s = 0.466\ ms$, and $P^*_{g_1} = 195.2\ MPa$.